PHOTONICS Research

Direct generation of an ultrafast vortex beam in a CVD-graphene-based passively mode-locked Pr:$LiYF_4$ visible laser

Nan Li,[1] Junjie Huang,[3] Bin Xu,[1,2,*] Yaqi Cai,[1] Jie Lu,[3] Linjie Zhan,[3] Zhengqian Luo,[1] Huiying Xu,[1] Zhiping Cai,[1] and Weiwei Cai[3]

[1]Department of Electronic Engineering, Xiamen University, Xiamen 361005, China
[2]Shenzhen Research Institute of Xiamen University, Shenzhen 518057, China
[3]Department of Physics, State Key Laboratory of Physical Chemistry of Solid Surfaces, Xiamen University, Xiamen 361005, China
*Corresponding author: xubin@xmu.edu.cn

Received 19 August 2019; revised 2 September 2019; accepted 2 September 2019; posted 4 September 2019 (Doc. ID 375725); published 4 October 2019

We report on the direct generation of passively mode-locked vortex lasers in the visible spectral region, for the first time to the best of our knowledge, using a Pr:$LiYF_4$ (Pr:YLF) crystal as the gain medium. A stable mode-locked TEM_{00} mode has been achieved with a maximum average output power of 75 mW using a graphene saturable absorber mirror. The mode-locked pulse width is measured to be as short as about 73.4 ps at a repetition rate of about 140 MHz, and the laser wavelength is at about 721 nm with spectral width of about 0.5 nm. By slightly misaligning the laser resonator, a first-order Laguerre-Gaussian mode ($LG_{0,1}$) has also been obtained with output power reduced to about 22 mW. The achieved $LG_{0,1}$ mode has been verified via a home made improved Fizeau interferometer. This work provides a simple and universal method for direct generation of an ultrafast vortex laser, which can be readily extended to other spectral regions by using different laser gain mediums.

https://doi.org/10.1364/PRJ.7.001209

1. INTRODUCTION

An optical vortex beam is a helical-phased light that possesses orbital angular momentum due to the phase singularity, which gives rise to a wide range of applications, such as quantum entanglement [1], optical tweezers [2], optical communications [3], optical testing [4], and material processing [5,6]. With the rising interest in optical vortex beams, presently, a variety of approaches have been demonstrated to generate vortex beams, including spiral phase plates [7], computer-generated holograms [8,9], *q*-plates [10,11], and astigmatic lenses [12,13].

An optical vortex beam operating in pulsed modes could be more advantageous for various applications, e.g., high-quality material processing [14] and controllable specificity of chiral matter [15], especially, an ultrashort pulsed vortex laser with picosecond or femtosecond pulse time duration that combines the advantages of an ultrafast laser and vortex laser. In fact, ultrafast optical vortices have shown tremendous potential in, for instance, ultrafast physical and chemical processes, ultrafast nonlinear spectroscopy, nanomachining, and terahertz vortex generation [16–18]. In 2017, Qiao *et al.* reported an extracavity ultrafast vortex laser by transforming the incident femtosecond Hermite–Gaussian (HG) mode into a corresponding LG mode outside the laser resonator via cylindrical lens mode converter [19].

Direct generation of a vortex beam from a laser cavity is advantageous in system simplicity and beam quality. However, at present, direct generation of an ultrafast vortex laser has been rarely reported. Recently, Wang *et al.* reported a SESAM mode-locked (ML) Yb:phosphate glass laser with 45.7 mW output power of an $LG_{0,1}$ vortex beam by off-axis pumping and astigmatism-induced Gouy phase difference between HG_{10} and HG_{01} modes [20]. After, the same group has also reported a SESAM mode-locked Yb:KYW laser using an intracavity defect-spot mirror [21]. However, direct generation of an ultrafast vortex laser has not yet been extended to other spectral regions, e.g., the important visible wavelength range. It is well known that a visible laser has crucial applications in color display, data storage, and medical imaging [22].

In terms of laser emission in the visible range, in fact, apart from the costly commercially available Ti:sapphire laser, an ultrafast visible laser is still in its initial stage, not to mention an ultrafast vortex visible laser. With the development of blue diode lasers, as the main sources, Pr^{3+}-doped visible lasers have attracted rising interest. In 2014, using an optically pumped semiconductor laser (OPSL) as a pump source, the first ultrafast

Pr^{3+}-doped visible laser at 639 nm via passively mode-locking technology was reported using a well-designed GaInP quantum well SESAM [23]. In 2016, the first diode-pumped passively mode-locked Pr^{3+}-doped visible laser was reported by Iijima *et al.* [24]. Recently, 2D materials acting as effective saturable absorbers (SAs), represented by graphene [25–27], MoS_2 [28,29], Bi_2Se_3 [30,31], black phosphorus [32–34], and perovskite nanosheets [35], have become a hot research topic because of their superior merits, e.g., broadband absorption as one of the main advantages, compared with those conventional saturable absorbers [36]. In 2017, Zhang *et al.* [29] reported broadband mode-locked Pr^{3+}-doped visible lasers at 522, 607, and 639 nm using MoS_2.

In this work, a chemical vapor deposition (CVD) graphene saturable absorber mirror (SAM) has been successfully fabricated. Using it for passive mode locking, we have operated a blue-diode-pumped Pr:YLF laser at 721 nm, for the first time to our knowledge. By slightly misaligning the laser resonator, an ultrafast vortex laser can also be directly generated from the Pr:YLF laser cavity.

2. EXPERIMENTAL DETAILS

Figure 1 shows the experimental setup of the blue diode-pumped mode-locked Pr:YLF laser. The laser crystal was pumped by two 4-W diode lasers emitting at about 444 nm from two ends of the laser resonator, which is believed to have better mode overlap between the pump beam and cavity mode than single-end pumping. At the same time, the double-end pumping geometry with higher pump power is also of advantage for operating the mode-locked laser at higher output power. During all the experiments, two focusing lenses, both with 75 mm focal length, were used to focus the pump beam into the laser crystal from the two sides. The four curved mirrors, M1–M4, have the same radii of curvature of 100 mm. M1–M3 have the same coating, i.e., high transmission at pumping wavelength and high reflection (>99.9%) at the considered lasing wavelength (721 nm). M4, used as output coupler, has a transmission of about 3.1% at 721 nm. Two layers of the CVD graphene have been transferred one by one onto a flat mirror (M5). The M5 has a high-reflection coating of more than 99.9% at 721 nm, thus forming a reflection-type graphene SAM.

The laser gain medium is an *a*-cut Pr:YLF crystal with a dopant concentration of 0.5 at% and dimensions of 3 mm × 3 mm × 5 mm. In order to protect the laser crystal from

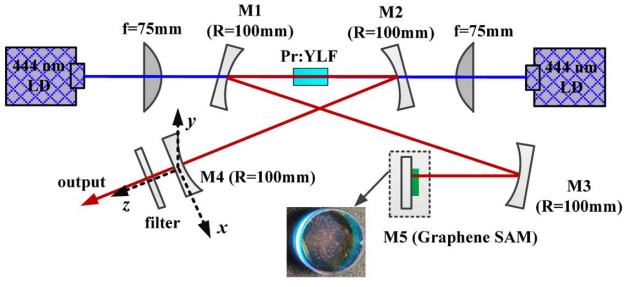

Fig. 1. Schematic of the graphene mode-locked Pr:YLF laser with total cavity length of about 106 cm (M1-M2: 13 cm, M2-M4: 27 cm, M1-M3: 59 cm, and M3-M5: 7 cm).

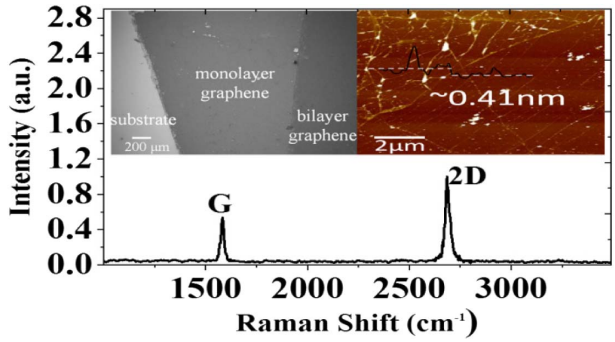

Fig. 2. Raman spectrum of the graphene excited by a 488 nm laser. Inset: SEM (left) and AFM (right) images of the CVD graphene.

thermal fracture, it was wrapped with indium foil and then mounted inside a copper block. The copper block was connected to a water-cooled chiller with temperature at 16°C during the laser experiment.

The SAM consisted of two layers of CVD graphene, which were transferred one by one onto a high-reflection dielectric flat mirror. The detailed transfer process can be found in many previous publications, e.g., Ref. [37]. To assess its quality, we measured the Raman spectrum of the as-fabricated graphene SAM with a 488 nm laser source, as shown in Fig. 2. The two characteristic Raman peaks of graphene, designated as G and 2D, can be clearly seen in the figure. The G-band peak in the Raman spectrum was located at ~1583 cm^{-1} with an FWHM of about 14 cm^{-1}, and the 2D-band peak was at ~2684 cm^{-1} with an FWHM of about 27 cm^{-1}. The D-band peak, which is related to defects, was not observed at ~1350 cm^{-1} after subtracting the Raman signal of a highly reflective mirror substrate. The indiscernible D-band peak confirms the presence of high-quality graphene of the CVD-grown graphene. Figure 2, as insets, also shows the scanning electron microscopy (SEM) and atomic force microscopy (AFM) images of the graphene. The result shows that the thickness of graphene is 0.41 nm, i.e., two layers of the sample.

3. RESULTS AND DISCUSSION

By focusing the pump beam right on the optical axis of the laser cavity and finely aligning the cavity, stable mode-locked Pr:YLF laser pulse train output can be observed with a visible GaAs photodetector (ET4000F with rise time <30 ps) and an oscilloscope (Agilent Infinium DSO81204A, 12 GHz,

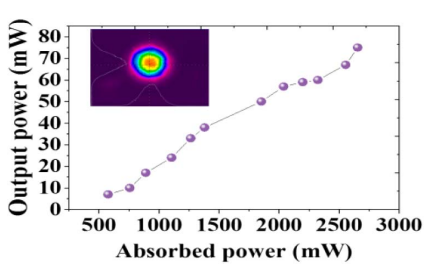

Fig. 3. Average output power versus absorbed power of mode-locked Pr:YLF laser at 721 nm.

40 GSa/s). Moreover, using a laser beam quality analyzer (Spiricon M^2–200), a TEM_{00} Gaussian fundamental mode was also observed. Figure 3 shows the dependence of the laser average output power on the absorbed power. Stable CW mode locking was achieved when the absorbed power was increased to about 552 mW, below which the laser showed unstable *Q*-switched mode locking. Increasing the absorbed power to about 2.65 W, we obtained a maximum average output power of 75 mW.

Spectra of the achieved CW and mode-locked lasers are both shown in Fig. 4(a), which were measured with an optical spectrum analyzer (Advantest Q8384 Optical Spectrum Analyzer) with a resolution of 0.08 nm. For both cases, the laser spectra are centered at about 721 nm with FWHMs of about 0.2 nm for CW operation and 0.5 nm for mode-locked operation. The emission spectrum of Pr:YLF crystal has a linewidth of about 1 nm at this 721 nm emission band (π polarization), which corresponds to a sub-ps pulse-width theoretically. Moreover, we measured the radio-frequency (RF) spectrum of the mode-locked pulses with a Gwinstek GSP-930 spectrum analyzer, as shown in Fig. 4(b). The RF spectrum shows a signal-to-noise ratio as high as 46 dB. According to the RF spectrum, the mode-locked pulses had a repetition rate of 140 MHz, which corresponds to the laser cavity length of about 1.1 m. Figure 4(c) shows the pulse trains on microsecond time scales (50 μs/div) of the continuous-wave mode-locked laser. The single-pulse profile is also shown in Fig. 4(d) with pulse time duration of 73.4 ps measured by the high-speed oscilloscope.

Noncollinear pumping, similar to off-axis pumping, is an effective way to realize the HG mode, as demonstrated in Ref. [19]. In fact, this kind of method can also be used for high-order HG modes generation, e.g., 28th order in the near-infrared wavelength band [38]. However, it is indeed possible to realize the LG mode directly from a laser cavity. Recently, we demonstrated direct generation of a continuous-wave vortex laser just by orthogonally rotating the laser gain medium to force noncollinear pumping in two orthogonal directions [39].

In this experiment, in order to realize a mode-locked Pr:YLF vortex laser, instead of rotating the laser gain medium, we orientated the output coupler (M4) in the *xz* plane at first. This step is similar to that reported in Ref. [19], and we also observed $HG_{0,1}$ mode generation. As we simulated in Ref. [39], under this situation, generation of the $HG_{0,1}$ mode should be explained by a lower threshold of the $HG_{0,1}$ mode than the $TEM_{0,0}$ mode because of the rotating induced destruction to the symmetry of the laser cavity. We further orientated the OC in the *yz* plane, namely, orthogonal to the *xz* plane, which is similar to our previous method, as reported in Ref. [39], for vortex generation. The orthogonal rotation of the OC leads to the formation of two petal beams, i.e., $HG_{0,1}$ and $HG_{1,0}$ modes, and the superposition of two petal beams will form a doughnut beam. During the generation of a vortex beam, a crucial factor is the introduction of $\pi/2$ Gouy phase. According to Ref. [20], the $\pi/2$ Gouy phase could be induced by the astigmatism of a curved mirror. In this experiment, orthogonally rotating the curved OC leading to an astigmatism effect more or less should answer for the vortex generation. It should be pointed out that this proposed method can also generate the high-order HG mode easily. However, at present, we are not able to convert the high-order HG mode into its corresponding high-order LG mode, and only $HG_{0,1}$ can be successfully converted into the $LG_{0,1}$ mode, as shown in this experiment. This is probably because the present Pr:YLF laser system does not support high-order vortex beam generation, which requires larger loss introduction.

Figure 5 depicts the average output power of an ML vortex laser as a function of absorbed pump power with a maximum output power of 22 mW at 2038 mW of absorbed power, while the laser threshold increased to more than 800 mW. Further increasing the pump power led to purity of the vortex beam degradation. The purity degradation of the vortex beam should be explained by thermally induced symmetry improvement of the laser cavity under the present cavity misalignment, which is prone to supporting low-order mode for the laser cavity. The vortex laser beam spot is shown in Fig. 5, as an inset, from which one can clearly see a doughnut beam. It can be further confirmed by the laser intensity distribution. However, as we know, such doughnut beam could be coherent or incoherent superposition of $HG_{0,1}$ and $HG_{1,0}$ modes. A doughnut beam formed by incoherent superposition leads to an obscure spiral pattern in the interference patterns. However, for coherent superposition of two petal beams, clear and stable helical

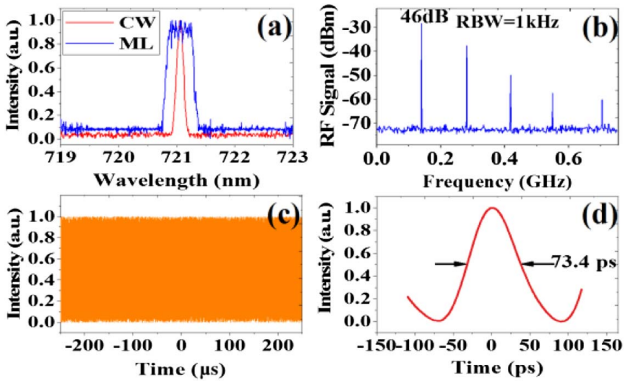

Fig. 4. (a) Spectra of CW and mode-locked lasers. (b) RF spectrum. (c) Typical mode-locked pulse trains. (d) Single pulse trace.

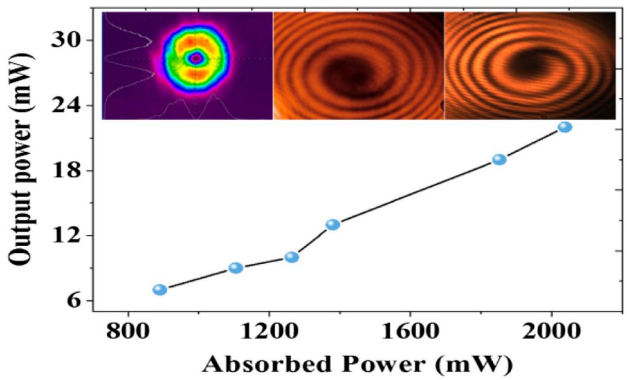

Fig. 5. Average output power versus absorbed power of the ML vortex laser. Inset: (left) vortex beam spot with intensity distribution curve, (middle) anticlockwise interference pattern, and (right) clockwise interference pattern.

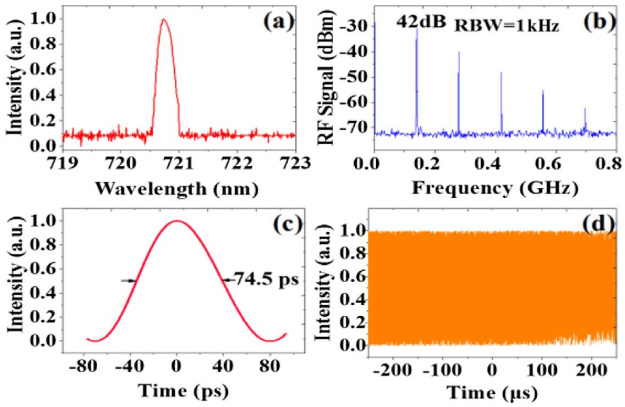

Fig. 6. (a) Optical spectrum of ML vortex. (b) Radio-frequency spectrum of ML vortex. (c) Single pulse trace of ML vortex. (d) Typical mode-locked pulse train on microsecond time scales.

wavefronts can be observed [40]. The interference pattern with well-determined handedness is shown as an inset in Fig. 5. Moreover, during the experiment, we found the helical stripe is stable, and no handedness change occurs. Further, the handedness shift can be readily realized by slightly moving the Pr:YLF crystal perpendicularly to the cavity axis, which indicated that moving the crystal led to spiral symmetry breakage.

Figure 6 shows the ultrafast vortex laser characteristics. The laser spectrum, as shown in Fig. 6(a), centered at 720.7 nm, has a linewidth of about 0.4 nm. Compared with the TEM_{00} mode laser, the present vortex laser has a wavelength blueshift of about 0.3 nm. This phenomenon should be explained by the increase of intracavity loss. The relatively narrowed linewidth of the vortex laser indicated less longitudinal modes inside the laser cavity because of an extra loss arising from cavity misalignment. Figure 6(b) shows the RF spectrum of the ultrafast vortex laser with a signal-to-noise ratio of 42 dB. The single-pulse profile and pulse trains are shown in Figs. 6(c) and 6(d), respectively. The pulse width is about 74.5 ps.

4. CONCLUSION

In conclusion, an ultrafast visible laser at about 720 nm has been achieved in a Pr:YLF laser using a graphene SAM. The pulse width was found to be about 73.4 ps. The average maximum output power reached 75 mW, which is believed to be the highest output power for a passively mode-locked Pr:YLF laser. Direct generation of an ultrafast vortex laser at this visible wavelength has also been realized with a maximum average output power of 22 mW and a pulse width of about 74.5 ps. This work has proposed a simple method for direct generation of an ultrafast vortex laser, which can be readily extended to other wavelength regions with different laser materials. In the near future, more than two layers of high-quality CVD graphene samples will be used for increasing the modulation depth of the SAM, which could realize shorter pulse width. Moreover, using a method for high-order vortex generation as proposed in Ref. [41], we hope that high-order ultrafast vortex lasers could be realized.

Funding. Natural Science Foundation of Fujian Province of China (2018J01108); National Natural Science Foundation of China (91750115); International Collaborative Laboratory of 2D Materials for Optoelectronics Science and Technology, Shenzhen University (2DMOST2018026).

REFERENCES

1. A. Mair, A. Vaziri, G. Weihs, and A. Zeilinger, "Entanglement of the orbital angular momentum states of photons," Nature **412**, 313–316 (2001).
2. K. T. Gahagan and G. A. Swartzlander, Jr., "Optical vortex trapping of particles," Opt. Lett. **21**, 827–829 (1996).
3. J. Wang, J.-Y. Yang, I. M. Fazal, N. Ahmed, Y. Yan, H. Huang, Y. Ren, Y. Yue, S. Dolinar, M. Tur, and A. E. Willner, "Terabit free-space data transmission employing orbital angular momentum multiplexing," Nat. Photonics **6**, 488–496 (2012).
4. P. Senthilkumaran, "Optical phase singularities in detection of laser beam collimation," Appl. Opt. **42**, 6314–6320 (2003).
5. K. Sueda, G. Miyaji, N. Miyanaga, and M. Nakatsuka, "Laguerre-Gaussian beam generated with a multilevel spiral phase plate for high intensity laser pulses," Opt. Express **12**, 3548–3553 (2004).
6. C. Hnatovsky, V. G. Shvedov, W. Krolikowski, and A. V. Rode, "Materials processing with a tightly focused femtosecond laser vortex pulse," Opt. Lett. **35**, 3417–3419 (2010).
7. M. W. Beijersbergen, R. P. C. Coerwinkel, M. Kristensen, and J. P. Woerdman, "Helical-wavefront laser beams produced with a spiral phase plate," Opt. Commun. **112**, 321–327 (1994).
8. N. R. Heckenberg, R. McDuff, C. P. Smith, and A. G. White, "Generation of optical phase singularities by computer-generated holograms," Opt. Lett. **17**, 221–223 (1992).
9. S. Ngcobo, I. Litvin, L. Burger, and A. Forbes, "A digital laser for on-demand laser modes," Nat. Commun. **4**, 2289 (2013).
10. L. Marrucci, C. Manzo, and D. Paparo, "Optical spin-to-orbital angular momentum conversion in inhomogeneous anisotropic media," Phys. Rev. Lett. **96**, 163905 (2006).
11. E. Karimi, B. Piccirillo, E. Nagali, L. Marrucci, and E. Santamato, "Efficient generation and sorting of orbital angular momentum eigenmodes of light by thermally tuned *q*-plates," Appl. Phys. Lett. **94**, 231124 (2009).
12. K. Dholakia, N. B. Simpson, M. J. Padgett, and L. Allen, "Second-harmonic generation and the orbital angular momentum of light," Phys. Rev. A **54**, R3742–R3745 (1996).
13. M. W. Beijersbergen, L. Allen, H. E. L. O. van der Veen, and J. P. Woerdman, "Astigmatic laser mode converters and transfer of orbital angular momentum," Opt. Commun. **96**, 123–132 (1993).
14. J. Hamazaki, R. Morita, Y. Kobayashi, S. Tanda, and T. Omatsu, "Laser ablation using a nanosecond optical vortex pulse," in *Proceedings of IEEE Conference on CLEO/Europe-EQEC* (IEEE, 2009), paper CC1.5THU.
15. D. L. Andrews, L. C. Dávila Romero, and M. Babiker, "On optical vortex interactions with chiral matter," Opt. Commun. **237**, 133–139 (2004).
16. G. F. Quinteiro and J. Berakdar, "Electric currents induced by twisted light in quantum rings," Opt. Express **17**, 20465–20475 (2009).
17. Y. S. Lee, *Principles of Terahertz Science and Technology* (Springer, 2009).
18. M. Bock, J. Jahns, and R. Grunwald, "Few-cycle high-contrast vortex pulses," Opt. Lett. **37**, 3804–3806 (2012).
19. Z. Qiao, L. Kong, G. Xie, Z. Qin, P. Yuan, L. Qian, X. Xu, J. Xu, and D. Fan, "Ultraclean femtosecond vortices from a tunable high-order transverse-mode femtosecond laser," Opt. Lett. **42**, 2547–2550 (2017).
20. S. Wang, S. Zhang, H. Yang, J. Xie, S. Jiang, G. Feng, and S. Zhou, "Direct emission of chirality controllable femtosecond LG_{01} vortex beam," Appl. Phys. Lett. **112**, 201110 (2018).
21. S. Wang, Z. Zhao, I. Ito, and Y. Kobayashi, "Direct generation of femtosecond vortex beam from a Yb:KYW oscillator featuring a defect-spot mirror," OSA Continuum **2**, 523–530 (2019).
22. G. Huber, T. Kellner, H. M. Kretschmann, T. Sandrock, and H. Scheife, "Compact diode pumped cw solid-state lasers in the visible spectral region," Opt. Mater. **11**, 205–216 (1999).

23. M. Gaponenko, P. W. Metz, A. Härkönen, A. Heuer, T. Leinonen, M. Guina, T. Südmeyer, G. Huber, and C. Kränkel, "SESAM mode-locked red praseodymium laser," Opt. Lett. **39**, 6939–6941 (2014).
24. K. Iijima, R. Kariyama, H. Tanaka, and F. Kannari, "Pr^{3+}:YLF mode-locked laser at 640 nm directly pumped by InGaN-diode lasers," Appl. Opt. **55**, 7782–7787 (2016).
25. Q. Bao, H. Zhang, Y. Wang, Z. Ni, Y. Yan, Z. X. Shen, K. P. Loh, and D. Y. Tang, "Atomic-layer graphene as a saturable absorber for ultrafast pulsed lasers," Adv. Funct. Mater. **19**, 3077–3083 (2009).
26. H. Zhang, D. Y. Tang, L. M. Zhao, Q. L. Bao, and K. P. Loh, "Large energy mode locking of an erbium-doped fiber laser with atomic layer graphene," Opt. Express **17**, 17630–17635 (2009).
27. Z. Sun, T. Hasan, F. Torrisi, D. Popa, G. Privitera, F. Wang, F. Bonaccorso, D. M. Basko, and A. C. Ferrari, "Graphene mode-locked ultrafast laser," ACS Nano **4**, 803–810 (2010).
28. B. Xu, Y. Cheng, Y. Wang, Y. Huang, J. Peng, Z. Luo, H. Xu, Z. Cai, J. Weng, and R. Moncorgé, "Passively *Q*-switched Nd:$YAlO_3$ nanosecond laser using MoS_2 as saturable absorber," Opt. Express **22**, 28934–28940 (2014).
29. Y. X. Zhang, H. H. Yu, R. Zhang, G. Zhao, H. J. Zhang, Y. X. Chen, L. M. Mei, M. R. Tonelli, and J. Y. Wang, "Broadband atomic-layer MoS_2 optical modulators for ultrafast pulse generations in the visible range," Opt. Lett. **42**, 547–550 (2017).
30. B. Xu, Y. Wang, J. Peng, Z. Luo, H. Xu, Z. Cai, and J. Weng, "Topological insulator Bi_2Se_3 based *Q*-switched Nd:$LiYF_4$ nanosecond laser at 1313 nm," Opt. Express **23**, 7674–7680 (2015).
31. Z. Dou, Y. Song, J. Tian, J. Liu, Z. Yu, and X. Fang, "Mode-locked ytterbium-doped fiber laser based on topological insulator: Bi_2Se_3," Opt. Express **22**, 24055–24061 (2014).
32. Y. Chen, G. Jiang, S. Chen, Z. Guo, X. Yu, C. Zhao, H. Zhang, Q. Bao, S. Wen, D. Tang, and D. Fan, "Mechanically exfoliated black phosphorus as a new saturable absorber for both *Q*-switching and mode-locking laser operation," Opt. Express **23**, 12823–12833 (2015).
33. S. B. Lu, L. L. Miao, Z. N. Guo, X. Qi, C. J. Zhao, H. Zhang, S. C. Wen, D. Y. Tang, and D. Y. Fan, "Broadband nonlinear optical response in multilayer black phosphorus: an emerging infrared and mid-infrared optical material," Opt. Express **23**, 11183–11194 (2015).
34. Z. Guo, H. Zhang, S. Lu, Z. Wang, S. Tang, J. Shao, Z. Sun, H. Xie, H. Wang, X. Yu, and P. Chu, "From black phosphorus to phosphorene: basic solvent exfoliation, evolution of Raman scattering, and applications to ultrafast photonics," Adv. Funct. Mater. **25**, 6996–7002 (2015).
35. P. Li, Y. Chen, T. Yang, Z. Wang, H. Lin, Y. Xu, L. Li, H. Mu, B. N. Shivananju, Y. Zhang, Q. Zhang, A. Pan, S. Li, D. Tang, B. Jia, H. Zhang, and Q. Bao, "Two-dimensional $CH_3NH_3PbI_3$ perovskite nanosheets for ultrafast pulsed fiber lasers," ACS Appl. Mater. Interfaces **9**, 12759–12765 (2017).
36. Y. Song, X. Shi, C. Wu, D. Tang, and H. Zhang, "Recent progress of study on optical solitons in fiber lasers," Appl. Phys. Rev. **6**, 021313 (2019).
37. X. Li, W. Cai, J. An, S. Kim, D. Yang, R. Piner, A. Velamakani, I. Jung, E. Tutuc, S. Banerjee, L. Colombo, and R. Ruoff, "Large-area synthesis of high-quality and uniform graphene films on copper foils," Science **324**, 1312–1314 (2009).
38. Y. F. Chen, T. M. Huang, C. F. Kao, C. L. Wang, and S. C. Wang, "Generation of Hermite-Gaussian modes in fiber-coupled laser-diode end-pumped lasers," IEEE J. Quantum Electron. **33**, 1025–1031 (1997).
39. X. Huang, B. Xu, S. Cui, H. Xu, Z. Cai, and L. Chen, "Direct generation of vortex laser by rotating induced off-axis pumping," IEEE J. Sel. Top. Quantum **24**, 1601606 (2018).
40. D. J. Kim and J. W. Kim, "Direct generation of an optical vortex beam in a single-frequency Nd:YVO_4 laser," Opt. Lett. **40**, 399–401 (2015).
41. Z. Qiao, G. Q. Xie, Y. Wu, P. Yuan, J. Ma, L. J. Qian, and D. Y. Fan, "Generating high-charge optical vortices directly from laser up to 288th order," Laser Photon. Rev. **12**, 1800019 (2018).